2010 International Symposium on Nonlinear Theory and its Applications
NOLTA2010, Krakow, Poland, September 5-8, 2010

A mathematical-structure-based aVLSI silicon neuron model

Takashi Kohno†‡ and Kazuyuki Aihara†

†Institute of Industrial Science, University of Tokyo
4-7-1 Komaba, Meguro-ku, Tokyo, 153-8505 Japan
‡PRESTO, Japan Science and Technology Agency
4-1-8 Honmachi, Kawaguchi-shi, Saitama, 332-0012 Japan
Email: kohno@sat.t.u-tokyo.ac.jp, aihara@sat.t.u-tokyo.ac.jp

Abstract—The mathematical structures under the conductance-based neuron models have been studied extensively from the perspective of the nonlinear dynamics and bifurcation theory. We proposed to design silicon neuron models by re-constructing the topological structures in the phase portraits and the bifurcation diagrams of the conductance-based neuron models utilizing device-native curves. It not only allows us to design simple circuitry retaining the neuronal dynamics but also provides effective procedures to determine the parameter voltages applied to operate the circuits. An analog Very-Large-Scale Integration (aVLSI) silicon neuron model that mimics the mathematical structures in two groups of bursting neurons was designed based on this idea. The results of the theoretical model and HSpice simulations are reported.

1. Introduction

The silicon neuron is an artificial copy of the neuronal cells made of electronic circuit, which is designed to simulate electrophysiological behavior in real time. Most of the silicon neurons are comprised of low-power consuming analog circuit that solves the models of neuronal cells. Implementing a detailed model of ionic conductances such as Leech heart interneuron model yields a silicon neuron circuit very similar to its biological counterpart [1]. However, such circuits, the conductance-based silicon neurons, reflect the complexity of the neuron models into their circuitry, which affects their stability, power consumption, and tunability of parameters. Particularly, the last point is a critical problem because these neuron models are dependent on large number of parameters and the characteristics of the circuit cannot be free from deviation. Some researchers adopt ultimately simple neuron models, the leaky integrate-and-fire model and its expansion, to resolve these problems [2], though it sacrifices the dynamical behavior of the silicon neurons, because such models describe limited aspects of the neuronal behavior.

In our previous works [3][4][5], we applied the techniques of qualitative modeling to design silicon neuron models that can be implemented by a simple and low-power consuming Metal-Oxide-Semiconductor Field-Effect Transistors (MOSFETs) circuit. These mathematical techniques have been studied over 50 years to elucidate the mechanisms of various neuronal behaviors utilizing the phase plane and the bifurcation analysis [6]. By reproducing such mechanisms utilizing the characteristics curves of MOSFET circuits, we can design device-native silicon neuron models that have the intrinsically same dynamics as the original neuron model. A silicon neuron model designed by this approach is presented in the following sections. It is designed to be implemented by differential pair and current-mode integrator circuitries operated in the subthreshold region of the MOSFET. These ultimately low-power-consuming circuitries are established and commonly utilized in conductance-based silicon neurons [1][7]. Another advantage to the simple circuitry and the preservation of dynamical behavior is that we can determine the parameter voltages adapting the variation of the circuit at fabrication by the mathematical techniques.

2. Design of system equations

The model of our silicon neuron is designed so that it copies the mathematical structures in two groups of bursting neurons, the square-wave and the elliptic bursters [8]. It had been elucidated that both of the bursters comprise a fast subsystem and a slow negative feedback current. The former is a basic excitable system that produces action potentials and the latter operates as an intrinsic stimulus to the former. The key property in these types of bursting is the bistability in the fast subsystem, which is produced by a saddle-loop homoclinic orbit bifurcation in the square-wave bursters and a subcritical Hopf bifurcation in the elliptic bursters. Our model re-constructs the topological structures in their phase portraits and bifurcation diagram.

The system equations of our silicon neuron model are as follows:

$$C_v \frac{dv}{dt} = -g(v) + f_m(v) - n - q + I_a + I_{stim}, \quad (1)$$

$$\frac{dn}{dt} = \frac{f_n(v) - n}{T_n}, \quad (2)$$

$$\frac{dq}{dt} = \frac{f_p(v) - q}{T_q}, \quad (3)$$

where n is a recovery variable and v and q respectively represent the membrane potential and the slow negative feed-

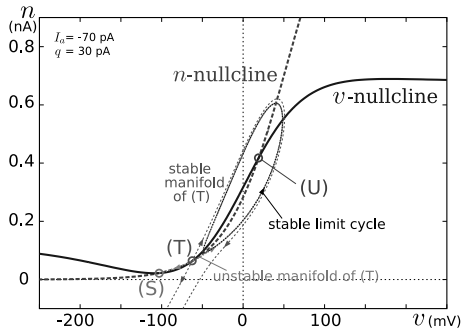

Figure 1: The n-v phase plane of the fast subsystem in our silicon neuron model in the square-wave burster mode. The value of q is near to and smaller than a saddle-loop homoclinic orbit bifurcation point.

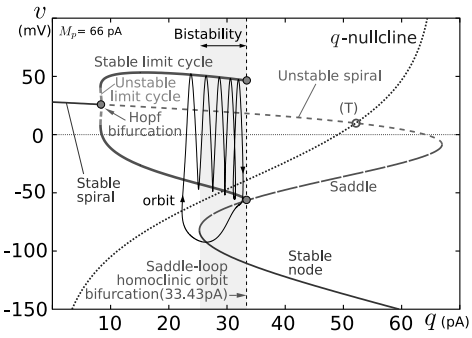

Figure 2: The v-q phase plane of our silicon neuron model in the square-wave burster mode. M_p = 66.0pA.

back that operates as an intrinsic stimulus current in parallel with an external one I_{stim} and a constant bias current I_a. The first two variables are the component of the fast subsystem. The time constants of the variables v, n, and q are represented by C_v, T_n, and T_q, respectively. The functions $g(v)$ and $f_x(v)$ (x=m,n,p) are the characteristic curves of differential-pair-based circuits. They are functions similar to the hyperbolic tangent as follows:

$$g(v) = S\frac{1-\exp(-\frac{\kappa}{U_T}(v-\theta)/2)}{1+\exp(-\frac{\kappa}{U_T}(v-\theta_y)/2)}, \quad (4)$$

$$f_x(v) = M_x\frac{1}{1+\exp(-\frac{\kappa}{U_T}(v-\delta_x))}, \quad (5)$$

where $x = m$, n, and p. In these equations, κ and U_T are respectively the capacitive coupling ratio and the thermal voltage, S and M_x are non-negative constants that control the amplitude of these functions, and θ and δ_x are constants that displace these functions in the direction of the v-axis.

2.1. Square-wave burster mode

When the parameters are selected appropriately, a saddle-loop homoclinic orbit bifurcation emerges in the

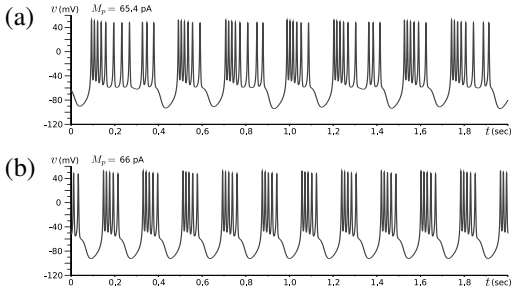

Figure 3: Time series of the membrane potential v. (a) chaotic bursting (M_p = 65.4 pA). (b) regular bursting (M_p = 66.0 pA). When M_p is smaller the system produces tonic or chaotic firing patterns (not shown).

fast subsystem when q is varied. The n-v phase plane near this bifurcation is drawn in Fig. 1. There exists a bistability between a stable limit cycle that represents a tonic firing state and a stable equilibrium ((S) in the figure) that represents a silent state. Figure 2 illustrates the bifurcation diagram of the fast subsystem where the bifurcation parameter is q, which draws the v-q plane of the whole system. When the system state is at the left (right) side of the q-nullcline, $\frac{dq}{dt}$ is positive (negative). This negative-feedback nature of q produces alternation between the tonic firing and the silent states where v is high and low, respectively. It is a mechanism of the burst firing. A trajectory of the state point is drawn in the figure (the closed curve labeled "orbit").

The waveforms of the membrane potential v are shown in Fig. 3, where (b) corresponds to the trajectory drawn in Fig. 2 and (a) shows a chaotic firing patterns observed when M_p is varied. In the previous work[5] we showed that our model produces chaotic firing patterns very similar to those reported both in a qualitative[9] and a biological models[10] of the square-wave burster. The fact that our model retains appropriately the ability to produce very complex firing patterns in the square-wave bursters supports that our model is their successful silicon-optimized model.

2.2. Elliptic burster mode

In this configuration, the parameters are selected so that the stable state loses stability via a subcritical Hopf bifurcation when q is decreased. The v-q plane of our silicon neuron model is drawn in Fig. 4. There is a unique stable equilibrium when q is sufficiently large and more than half part of the limit cycle is at the left side of the q-nullcline. Accordingly, q operates as a slow negative feedback current, which produces burst firing whose trajectory is drawn in the figure (the closed curve labeled "orbit"). The waveform of the membrane potential v that corresponds to this trajectory is shown in Fig. 5.

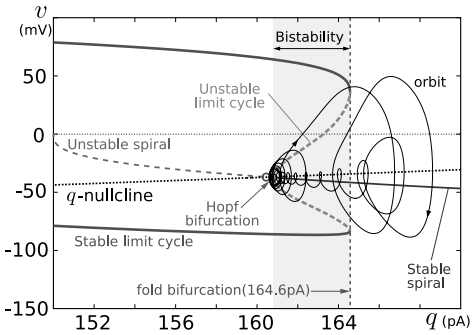

Figure 4: The v-q phase plane of our silicon neuron model in the elliptic burster mode. The stability of the unique equilibrium is inverted when q passes the Hopf bifurcation point. There exists bistability when q is between the Hopf bifurcation and the fold bifurcation points.

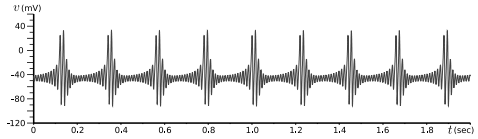

Figure 5: Time series of the membrane potential v.

3. Circuit Design and Parameter Tuning

The silicon neuron model designed in the previous section is implemented by a circuit whose block diagram is shown in Fig. 6. The circuitries of the blocks $f_x(v)$ and $g(v)$ are composed of differential pairs and current mirrors (Fig. 7). Integration of the variables n and q are realized by current-mode integrator circuits, whose circuitry is shown in Fig. 8. Their output currents I_n and I_q and the voltage of the capacitor C_v correspond to n, q, and v in the system equations, respectively.

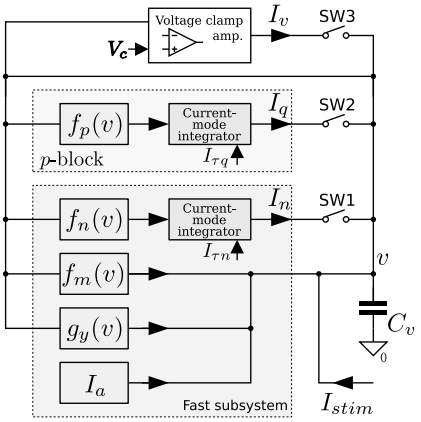

Figure 6: Block diagram of a silicon neuron circuit that implements our model.

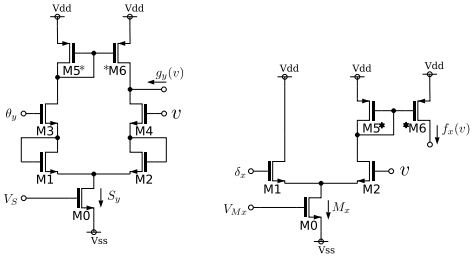

Figure 7: Schematics of the differential pair circuits for (a) $g(v)$ and (b) $f_x(v)$ (x = m, n, and p) in our silicon neuron model. The currents S and M_x are determined by the externally applied voltages V_S and V_{Mx}, respectively.

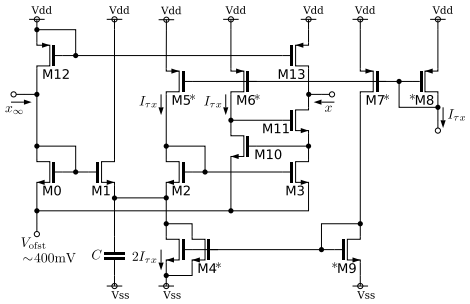

Figure 8: Schematic of the current-mode integrator in our circuit. The output current I_x is the temporal integration of $x_\infty - I_x$, where x_∞ is the input current. The time constant is determined by the capacitance C and the current $I_{\tau x}$. The terminal $V_{\rm ofst}$ is connected to a constant voltage source.

The three switches and the feedback amplifier (SW1–3 and Voltage clamp amp. in Fig. 6) allow us to make voltage clamp measurement. For the normal operation as a silicon neuron, SW1 and SW2 are turned on and SW3 is off . If SW1 and SW2 are turned off and SW3 is on, the membrane potential v is fixed to V_c by injection of I_v . The currents I_v, I_n, and I_q at the stationary state are measured for each V_c value, which draw the v-, n-, and q-nullclines, respectively. The n-v phase plane of the fast subsystem is drawn by combination of the first two nullclines. Because their topological structures, not exact shape, are responsible to the system's dynamics, we can determine the externally applied parameter voltages viewing the n-v phase plane structures dependent on the deviation of the circuits. Once the fast subsystem has set up, we can determine the parameter voltages for the slow feedback by drawing a part of the v-q plane. When SW1 is turned on and SW2 and SW3 are off, the fast subsystem operates independent of I_q. Because $-I_{stim}$ is equivalent to I_q, the stable structures of the v-q plane are drawn by plotting v for each I_{stim} value while decreasing and increasing it. We performed HSpice simulation utilizing TSMC CMOS .35μm mixed signal process PDK. Figure 9 shows an example v-q plane drawn in

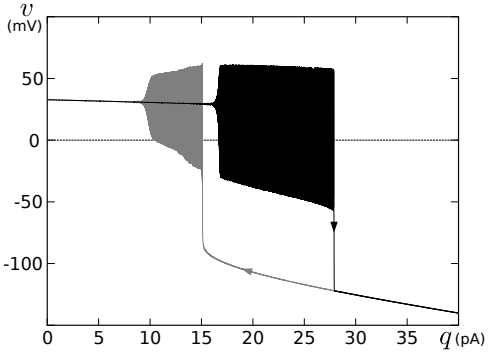

Figure 9: The *v*-*q* plane drawn in the HSpice simulation (corresponds to Fig. 2).

the simulation, where the two filled regions represent stable limit cycle. We can presume that there exists a stable limit cycle between them, and the Hopf bifurcation point is on the left edge of the right one. According to the procedures described above, we succeeded to find appropriate parameter sets for both of the square-wave and the elliptic burster modes. Total power consumption was estimated to be lower than 20 nW. In Fig. 10(a) and (b), the transient simulation results are shown that closely resemble the theoretical simulation results of the model shown in Fig. 3. We also succeeded to find a parameter set for the elliptic burster mode (Fig. 10(c)) in HSpice simulation.

4. Conclusion

We proposed a mathematical-structure-based approach, a new strategy for designing silicon neuron circuits based on the mathematical techniques. It not only allows us to design simple circuitry retaining the neuronal dynamics but also provides powerful theoretical procedures to determine the parameter voltages to realize an intended dynamics. This is demonstrated by a silicon neuron circuit designed according to this strategy that can be configured into two bursting modes, the square-wave and the elliptic burster modes. Though we could not describe because of space limitations, our circuit can be configured to copy the dynamics in the non-bursting neuron models, either the Class I or II in the Hodgkin's classification by turning SW2 off. If a slow variable is added that can be implemented by the same circuitry as *q*, our silicon neuron can produce dynamics of the parabolic burster [8] (Fig. 10(d)), another group of bursting neurons including Aplysia R15 cell.

Acknowledgments

The study was supported by JST PRESTO program and was partially supported by a Grant-in-Aid for Young Scientists (A) 19680015 from the Ministry of Education, Culture, Sports, Science, and Technology, the Japanese Government.

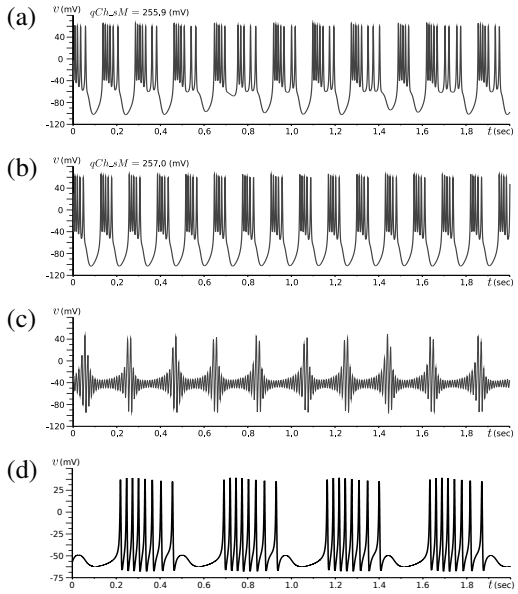

Figure 10: HSpice transient simulation results. (a) and (b) are in the square-wave burster mode (respectively correspond to Fig. 3(a) and (b)). (c) is in the elliptic burster mode. (d) is in the parabolic burster mode that are realized by adding another slow variable.

References

[1] M. F. Simoni, G. S. Cymbalyuk, M. E. Sorensen, R. L. Calabrese, and S. P. DeWeerth, "A multiconductance silicon neuron with biologically matched dynamics," *IEEE Transactions on Biomedical Engineering*, vol. 51, no. 2, pp. 342–354, Feb. 2004.

[2] G. Indiveri, "A low-power adaptive integrate-and-fire neuron circuit," in *Proceedings of IEEE International Symposium on Circuits and Systems*, vol. 4, no. IV, May. 2003, pp. 820–823.

[3] T. Kohno and K. Aihara, "A design method for analog and digital silicon neurons –mathematical-model-based method–," *AIP Conference Proceedings*, vol. 1028, pp. 113–128, Jul. 2008.

[4] M. Sekikawa, T. Kohno, and K. Aihara, "An integrated circuit design of a silicon neuron and its measurement results," *Journal of Artificial Life and Robotics*, vol. 13, no. 1, pp. 116–119, Dec. 2009.

[5] T. Kohno and K. Aihara, "A hindmarsh-rose type silicon neuron," in *Proceedings of the 3rd International Conference on Complex Systems and Applications*, Jun. 2009, p. 197.

[6] J. Rinzel and G. B. Ermentrout, "Analysis of neural excitability and oscillations," in *Methods in Neural Modeling*, 2nd ed., C. Koch and I. Segev, Eds. MA: MIT Press, 1998, ch. 7, pp. 251–291.

[7] Q. Zou, Y. Bornat, S. Saïghi, J. Tomas, S. Renaud, and A. Destexhe, "Analog-digital simulations of full conductance-based networks of spiking neurons with spike timing dependent plasticity," *Network: Computation in Neural Systems*, vol. 17, no. 3, pp. 211–233, Sep. 2006.

[8] X.-J. Wang and J. Rinzel, "Oscillatory and bursting properties of neurons," in *The Handbook of Brain Theory and Neural Networks*, 2nd ed., M. A. Arbib, Ed. MA: MIT Press, 2003, pp. 835–840.

[9] X.-J. Wang, "Genesis of bursting oscillations in the Hindmarsh-Rose model and homoclinicity to a chaotic saddle," *Physica D*, vol. 62, no. 1–4, pp. 263–274, Jan. 1993.

[10] T. R. Chay, "Electrical bursting and luminal calcium oscillation in excitable cell models," *Biological Cybernetics*, vol. 75, no. 5, pp. 419–431, Nov. 1996.